Hindawi Publishing Corporation
International Journal of Polymer Science
Volume 2016, Article ID 2081734, 9 pages
http://dx.doi.org/10.1155/2016/2081734

Research Article

Attapulgite Nanofiber-Cellulose Nanocomposite with Core-Shell Structure for Dye Adsorption

Xiaoyu Chen, Xiaoxue Song, and Yihe Sun

School of Material Engineering, Jinling Institute of Technology, Nanjing 211169, China

Correspondence should be addressed to Xiaoyu Chen; chxy@jit.edu.cn

Received 25 March 2016; Revised 22 May 2016; Accepted 31 May 2016

Academic Editor: Ming Zhang

Nanocomposite particle used for adsorption has attracted continuous attention because of large specific surface area and adjustable properties from nanocomponent. Herein nanocomposite particle with cellulose core and attapulgite nanofibers shell was prepared. The size of cellulose core was about 2 mm and the thickness of nanofibers shell is about 300 μm. Adsorption capacity of nanocomposite particle to methylene blue can reach up to 11.07 mg L^{-1} and the best adsorption effect occurs at pH = 8; pseudo-first-order equation and the Langmuir equation best describe the adsorption kinetic and isotherm, respectively; repeated adsorption-desorption experimental results show that 94.64% of the original adsorption capacity can be retained after being reused three times.

1. Introduction

Attapulgite nanofiber is a kind of hydrated octahedral layered magnesium aluminum silicate with diameter of 20 nm and length of several hundred nanometers to several micrometers [1, 2]. Theoretical formula of attapulgite nanofiber is $(Al_2Mg_2)Si_8O_{20}(OH)_2(OH_2)_4{\cdot}4H_2O$ [3]. Due to large specific surface area, attapulgite nanofiber has high sorption ability and is widely used in decoloring, drying, removing heavy metal ions or organic contaminants, and other fields [4, 5]. Attapulgite nanofiber possesses permanent negative charges and exchangeable cations [2]. Used as dye adsorbent, attapulgite nanofiber can remove cationic dye such as methylene blue from water. But when added to water, attapulgite nanofibers suspend in water and are difficult to be separated from water after adsorption. The suspended attapulgite will cause secondary pollution to the water and cannot be reused [6]. Therefore, finding an excellent carrier for attapulgite is important to avoid secondary pollution and to reuse attapulgite.

Polymer nanocomposites are composites of particle-filled polymers for which at least one dimension of the dispersed particles is in the nanometer range [7–9]. Polymer nanocomposites containing attapulgite nanofiber have been prepared, in which polymer exists as hydrogel and attapulgite nanofibers are embedded in the hydrogel [10, 11]. This hydrogel can be used as super adsorbent and adsorbent for heavy metal ions [10, 11].

Adsorption usually occurred on the surface of absorbent [12, 13]. Particle adsorbents have large surface area, which leads to high adsorption ability. Core-shell structure with adsorbent on the shell has low cost and is favorable for particle adsorbent to adsorb dye. Cellulose is one of the most abundant biopolymers in nature [14, 15]. Nanocomposite particle with cellulose core and attapulgite nanofiber shell has never been reported. But cellulose is difficult to dissolve in common solvent to form cellulose bead. NaOH/urea solution is a "green" and cheap method to dissolve cellulose with no pollution [16].

In this study, we combined attapulgite nanofiber and cellulose to prepare a low-cost adsorbent for water treatment. We prepared cellulose bead by dissolving cellulose in NaOH/urea solution as core to afford necessary strength. Attapulgite nanofibers were coated on cellulose bead as shell to adsorb dye. Coated attapulgite shell can prevent second pollution of attapulgite in water. The structure, adsorption

behaviors, and reusability of this nanocomposite were investigated.

2. Materials and Methods

2.1. Materials. NaOH, HCl, $CaCl_2$, urea, acetic acid, methylene blue (methylthioninium chloride $C_{16}H_{18}N_3SCl$), and other reagents used in the current work are all A.R. grade reagents. Attapulgite is provided by Jiangsu dianjinshi Au soil Mining Industry Co., Ltd. Distilled water is used in all experiments. Scoured cotton was used in this study as cellulose provided by Xuzhou weicai hygiene material factory Co., Ltd. Sodium alginate is provided by Shanghai Qingxi Chemical Technology Co., Ltd.

2.2. Preparation of the Nanocomposite Particle. Cellulose was dissolved in NaOH/urea solution using reported method [17]. Solution of NaOH (7 g), urea (12 g), and H_2O (81 mL) was cooled to −12°C; then 2 g scoured cotton was immediately added to above solution; then scoured cotton was stirred vigorously for 2 min to obtain a transparent cellulose solution. The resulting solution was dropped into 20 wt% acetic acid solution to form cellulose bead; then the cellulose bead was immersed in water for three days to remove urea and NaOH in bead.

Attapulgite powder was dispersed in 2.5 wt% sodium alginate solutions with agitation and the mass ratios of sodium alginate/attapulgite are 1 : 0, 1 : 1, 0.83 : 1, and 0.5 : 1. Then cellulose bead was coated with above suspension and dipped in $CaCl_2$ solution to cross-link the sodium alginate. The coated bead was washed with deionized water and dried in an oven at 50°C for 48 h to get dried composite particle. Composite particles with alginate/attapulgite mass ratios of 1 : 0, 1 : 1, 0.83 : 1, and 0.5 : 1 were labeled as AC0, AC1, AC2, and AC3, respectively. In addition, attapulgite and cellulose solution mixture was dropped into 20 wt% acetic acid solution to form bead coded as AC4.

2.3. Morphology and Structure of Composite Particle. Surface morphology of composite bead was observed by scanning electron microscopy (SEM, SU8010, Hitachi). Microstructure of composite particles was observed by digital microscope (503+ Guangzhou Haote optical instrument company). Fourier-transform infrared (FTIR) spectra are recorded by Smart iTR accessory of FTIR spectrometer (Thermo Fisher Nicolet iS10). Wide-angle X-ray diffraction (XRD) measurement was carried out on an XRD diffractometer (D8-Advance, Bruker). The patterns with the Cu Kα radiation at 40 kV and 30 mA were recorded in the region of 2θ from 5° to 70°. TGA (STA 409 PC Luxx NETZSCH) was performed by heating samples to 700°C at 5°C/min under a nitrogen flow.

2.4. Adsorption Studies

2.4.1. The Adsorption Ability Study. 0.1 g adsorbent was immersed into 80 mL methylene blue solution of 12.016 mg L^{-1} at 25°C for 36 h with 120 r/min controlled by a full temperature incubator shaker. The adsorption capacity Q (mg g^{-1}) was calculated using the following equation:

$$Q = \frac{(C_0 - C_e)V}{m}, \quad (1)$$

where C_0 (mg L^{-1}) is the initial dye concentrations of the solutions, C_e (mg L^{-1}) is the equilibrium dye concentrations of the solutions, V (L) is the volume of the solution, and m (g) is the dried weight of the adsorbent [18]. Methylene blue concentration was measured at 664 nm using UV-Vis spectrophotometer (VARIAN Cary 50).

2.4.2. pH Variation. The initial pH of methylene blue solution (12.016 mg L^{-1}) was adjusted by 0.1 mol L^{-1} HCl or NaOH aqueous solutions to change between 2.06 and 9.93. 0.1 g AC2 was immersed into 80 mL of above solution for 36 h at 25°C. The adsorption capacity was calculated based on (1).

2.4.3. Adsorption Kinetics. The change of adsorption capacity with time was measured. 0.5 g adsorbents (AC1) were immersed into 200 mL methylene blue solution of 12.016 mg L^{-1} at 25°C with continuous shaking at 120 r/min. At desired time intervals, 0.5 mL dyes solution was taken out to detect the current methylene blue concentration and 0.5 mL distilled water was added to the bulk solution to keep the volume constant. At time t_i, the adsorption capacity $Q(t_i)$ (mg g^{-1}) was calculated using the following equation [18]:

$$Q(t_i) = \frac{\left(C_0 - C_{t_i}\right)V_0 - \sum_2^{i-1} C_{t_{i-1}} V_S}{m}, \quad (2)$$

where C_{t_i} (mg L^{-1}) is the dye concentration at time t_i; V_S is the volume of solution taken out each time for dye concentration analysis, and m (g) represents the mass of the adsorbent [18].

2.4.4. Adsorption Equilibrium Study. 0.1 g of AC2 was immersed into 80 mL methylene blue solution with concentration of 6.008 mg L^{-1}, 9.012 mg L^{-1}, 10.514 mg L^{-1}, 12.016 mg L^{-1}, and 15.02 mg L^{-1}. Above five solutions were shook at 120 r/min at 25°C for 36 h. Then the adsorption capacity (Q_e) of each solution was measured based on (1). The same procedure was conducted at 30°C, 35°C, 40°C, and 50°C. Then the curves of Q_e-C_e were plotted.

2.5. Reusability Property. The methylene blue-loaded AC1 and AC2 were immersed into 0.1 mol L^{-1} H_2SO_4 aqueous solutions, washed with distilled water, and then reused in the next cycle of adsorption experiment. The adsorption-desorption experiments were conducted for four cycles. All experiments were performed at 25°C.

3. Results and Discussion

3.1. Preparation of Composite Particles. When used as adsorbent, attapulgite nanofiber usually suspends in solution,

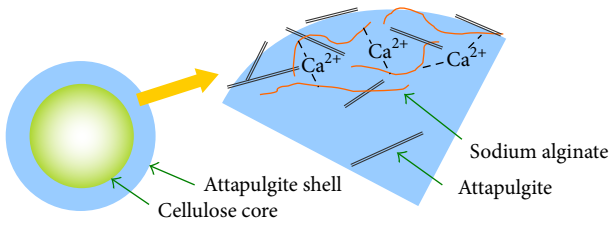

Figure 1: Schematic depiction of core-shell structure of cellulose-attapulgite composite particle.

which leads to second pollution to water and difficulty of regeneration. In this study, attapulgite is mixed with sodium alginate solution and is coated on the surface of cellulose bead. Sodium alginate, derived primarily from brown seaweed, is a linear polysaccharide copolymer that consists of two sterically different repeating units, β-D-mannuronic acid (M) and α-L-guluronic acid (G), in varying proportions [19]. Sodium alginate can be cross-linked by Ca^{2+} to form hydrogel. Above mixture is cross-linked by Ca^{2+} to form a hydrogel layer above the cellulose bead. After drying, the hydrogel becomes an attapulgite shell on the surface of cellulose core, preventing the second pollution of attapulgite powder. The structure of nanocomposite particle is shown in Figure 1.

Cellulose is selected to prepare the core for its low cost and being nontoxic and biodegradable. But cellulose is difficult to dissolve in usual solvent. In this study, we use NaOH/urea solution in low temperature as solvent to dissolve cellulose and to prepare cellulose bead as the core.

3.2. Morphology and Structure of Composite Particles. Figure 2(a) shows microscope image of AC2 and particle has a diameter of about 2 mm and has a core-shell structure. Figures 2(b)–2(f) show the SEM image of cross section and surface of composite particle. Figure 2(b) shows that the shell is adhered closely to the cellulose core and no obvious boundary is found. Figure 2(c) shows the coarse shell with thickness of 300 μm (area between two white arrows). Figure 2(d) shows the aggregation area of attapulgite nanofibers (white arrow pointed). Aggregation areas of attapulgite indicate that the dispersion of attapulgite in shell is not well. The aggregation areas are enlarged in Figure 2(e), from which fibrous attapulgite is found. Figure 2(f) shows the pure sodium alginate area existing in the shell.

FTIR spectra of sodium alginate, attapulgite, and AC2 are shown in Figure 3. In the spectrum of AC2, 1421 cm^{-1} belongs to the symmetric stretch vibration of C=O of sodium alginate. 3614 cm^{-1} is attributed to the stretching modes of hydroxyls coordinated with the magnesium. 3582 cm^{-1} and 3553 cm^{-1} belong to the symmetric and antisymmetric stretching mode of molecular water coordinated with the magnesium at the edges of the channels [20]. 1027 cm^{-1} belongs to Si-O-Si stretching vibration of attapulgite [21]. The results indicate that the shell is composed by sodium alginate and attapulgite. Smart iTR measures the surface structure of sample. So only the shell structure of composite particle can be detected.

Figure 4 shows the XRD peaks of attapulgite and attapulgite shell. Strong diffraction peak of 8.48° is a typical peak of attapulgite corresponding to basal spacing of about 10.55 Å and is attributed to the primary diffraction of the (110) crystal face. Other diffraction peaks are attributed as d(110) (10.55 Å), d(200) (6.43 Å), d(130) (5.43 Å), d(040) (4.48 Å), d(121) (4.14 Å), and d(061) (2.55 Å) [22]. All belong to the character peaks of attapulgite. The diffraction peaks of 26.54° are attributed to intergrowth minerals of quartz in attapulgite. In attapulgite shell, no obvious shift of peak position indicates that the crystal structure of attapulgite has no change during mixing. Absence of diffraction peaks of sodium alginate revealed that sodium alginate exists as amorphous. XRD results confirmed that attapulgite is the main component of shell.

TG and DTG curves for the cellulose, attapulgite, and AC1 are presented in Figure 5. The weight loss rate of AC1 is between attapulgite and cellulose. For AC1, below 100°C, the weight loss was ascribed to the removal of water which included surface water and zeolitic water of attapulgite. Between 200 and 300°C, the rapid weight loss can be attributed to the decomposition of cellulose and sodium alginate. Above 300°C, the weight loss corresponds to the degradation of residual decomposition products and loss of coordinated water and structural hydroxyl water in attapulgite [23]. The high residue mass of AC1 compared to the cellulose indicates the existence of attapulgite.

3.3. Adsorption Capacity. Figure 6 shows the adsorption effect of AC1 (Figure 6(a), before adsorption; Figure 6(b), after adsorption). The slight color of Figure 6(b) reveals that the nanocomposite particles could effectively remove the methylene blue from water. The clear solution indicates that attapulgite nanocomposite prevents the second pollution of attapulgite nanofiber in water.

Figure 7 compares the adsorption capacities of nanocomposite particles (AC1, AC2, and AC3) with core-shell structure to contrast samples (cellulose bead, AC0, and AC4). Composite particles have better adsorption capacities compared to the adsorption capacities of cellulose bead, AC0, and AC4, which indicate that the shell of attapulgite nanofiber can effectively absorb methylene blue. The adsorption capacities of AC1, AC2, and AC3 are higher than AC0 which only has a shell of sodium alginate, indicating the adsorption mainly resulted from attapulgite nanofiber. AC3 has maximum adsorption capacity of 9.1 $mg \cdot g^{-1}$.

Attapulgite fiber is a kind of silicate with nanosized rod-like morphology and consists of two double chains of the pyroxene type $(SiO_3)^{2-}$ like amphibole $(Si_4O_{11})^{6-}$ running parallel to the fiber axis [24, 25]. Attapulgite fiber has high surface area and moderate cation exchange capacity, which is useful for attapulgite as adsorbents to remove dye in wastewater. In addition, attapulgite fiber has negatively charged sorption sites because of isomorphic substitutions in structure. So attapulgite nanofiber can absorb cationic dyes through electrostatic attraction. The higher adsorption capacity of AC3 resulted from the high content of attapulgite nanofiber. From Figure 8, we can see that AC1 has rare

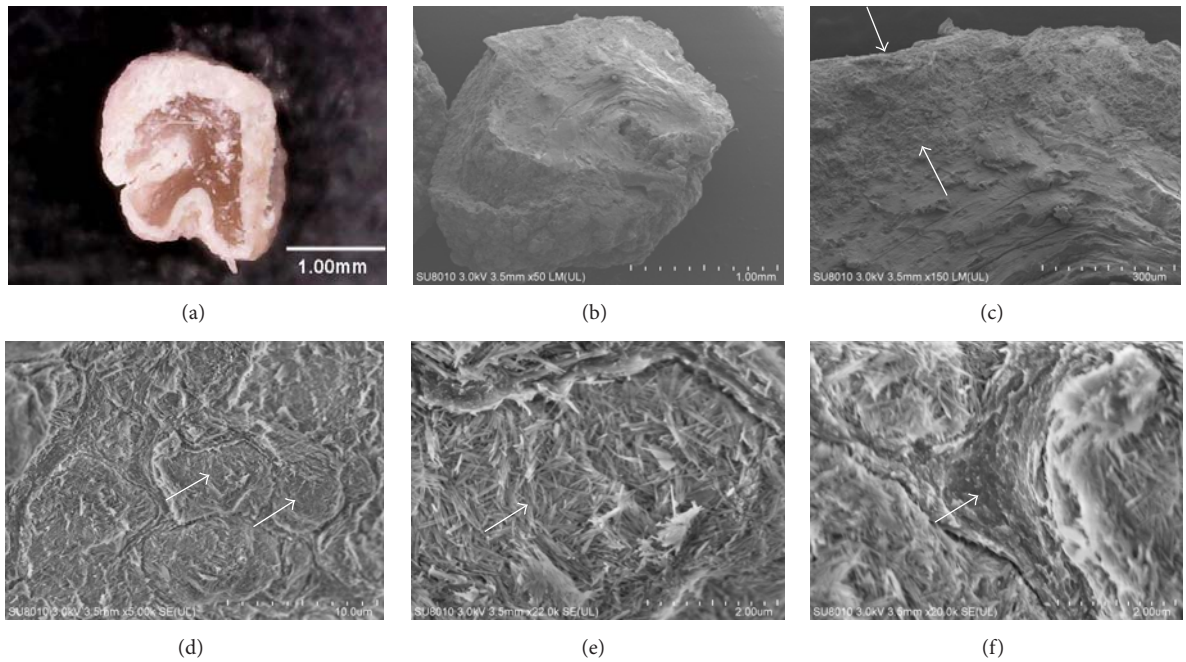

Figure 2: The morphology of the cellulose-attapulgite composite particles (AC2) ((a) cross section of particle by digital microscope; (b) cross section of particle by SEM; (c) shell structure of particle; (d) aggregation area of attapulgite; (e) amplified aggregation area of attapulgite; (f) area of sodium alginate).

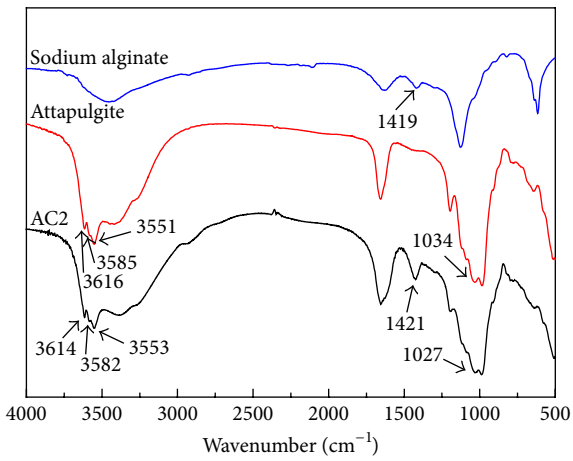

Figure 3: FTIR spectra of sodium alginate, attapulgite, and AC2.

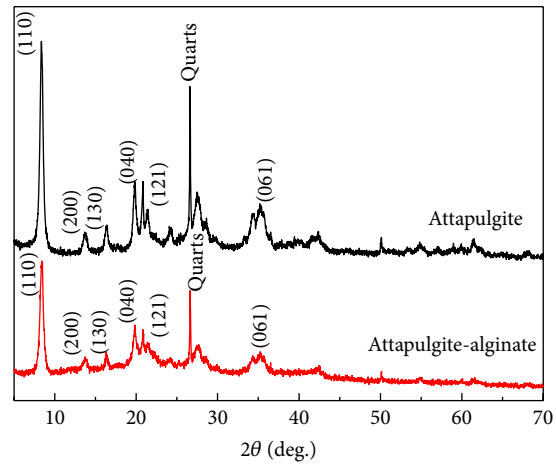

Figure 4: The powder X-ray diffraction pattern of the attapulgite and attapulgite shell.

dispersion of attapulgite nanofibers on the shell compared to AC2 and AC3, which leads to low adsorption capacity of AC1.

Other adsorption capacities for methylene blue have been reported, such as cross-linked porous starch (9.46 mg g^{-1}) [26], sugar extracted spent rice biomass (8.13 mg g^{-1}) [27], and attapulgite (51 mg g^{-1}) [28]. Compared to attapulgite, the relative lower capacity of nanocomposite particle may have resulted in the aggregation of attapulgite on the shell which was observed by SEM photo (Figure 2(d)). The aggregation decreased the specific surface area of attapulgite and then decreased adsorption ability [29].

3.4. Effects of pH on the Adsorption. Figure 9 shows the adsorption capacity of AC2 in the pH range of 2.06~9.93. As the pH increased from 2.06 to 7.97, adsorption capacity increased from 7.70 to 8.88 mg g^{-1}; as the pH increased from 7.97 to 9.93, adsorption capacity decreased from 8.88 to 8.43 mg g^{-1}.

For attapulgite, some isomorphic substitutions in the tetrahedral layer, such as Al^{3+} for Si^{4+}, develop negatively charged sorption sites (Si-O$^-$) on the surface of attapulgite [30]. Si-O$^-$ can absorb cation dye through electrostatic attraction [30]. But, at low pH, these negatively charged

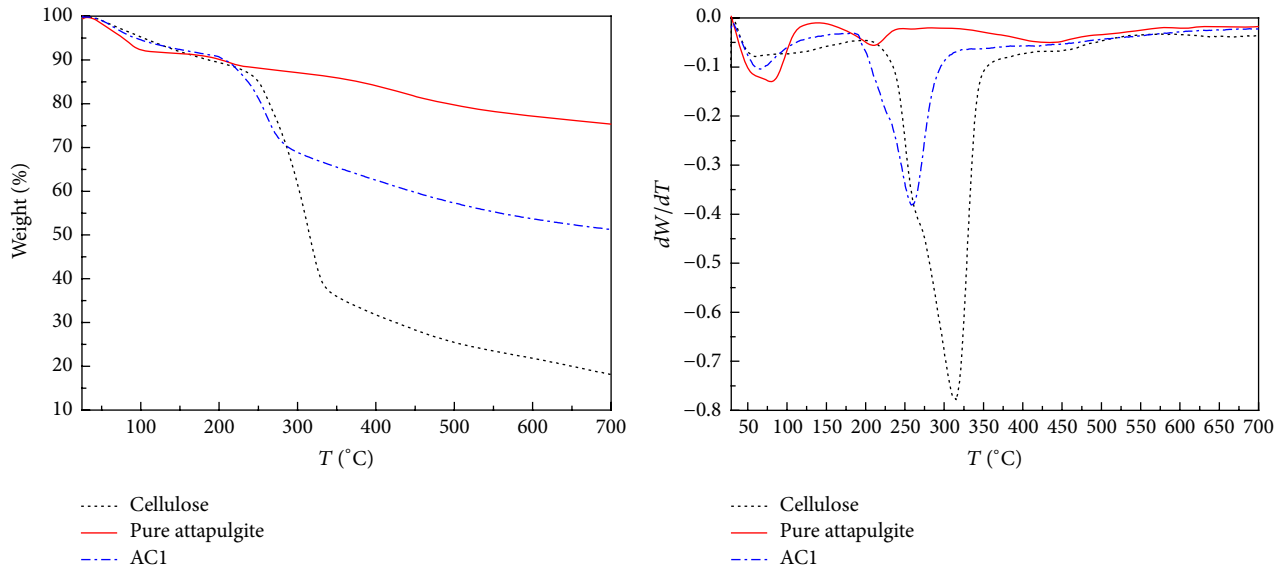

Figure 5: The TG and DTG of cellulose, attapulgite, and AC1.

Figure 6: The methylene blue adsorption effect of 0.5 g AC1 in 200 mL 12.016 mg L^{-1} methylene blue solution for 48 h ((a) before adsorption and (b) after adsorption).

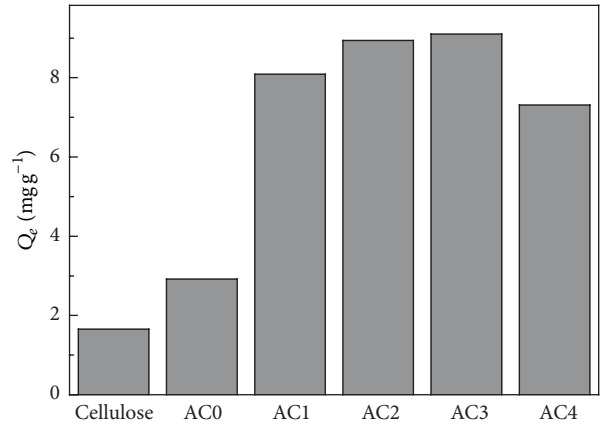

Figure 7: Adsorption capacity of six samples (cellulose bead, AC0, AC1, AC2, AC3, and AC4).

sorption sites are protonated to form Si-OH_2^+ by H^+, which decrease the negative sites to attract methylene blue. As pH increases, protonated groups become less and negatively charged sites such as Si-O^- increase and favor the adsorption of cationic dye. In the alkaline pH range, the decreasing of adsorption capacity could be attributed to competition of Na^+ ions for the negative adsorption sites [31].

3.5. Adsorption Kinetics. Time dependence of the adsorption capacity of AC1 for methylene blue was tested to study the adsorption kinetics. The initial concentration of methylene blue is 12.016 mg L^{-1}. The experimental results are shown in Figure 10. About 50% of methylene blue was adsorbed within 7 h. The adsorption equilibrium was achieved after 36 h. These results were similar to cross-linked porous starch whose adsorption equilibrium was reached in about 30 h for methylene blue [26].

To further investigate the adsorption mechanisms, four common kinetic models were used to fit the data, namely, pseudo-first-order model [32], pseudo-second-order model [33], intraparticle diffusion models [34], and the Elovich equation [35]. Table 1 shows the equations of these models. In these models, k_1 is the rate constant first-order absorption (min^{-1}) [32]; Q_{eq} (mg g^{-1}) is the amount of dye adsorbed at equilibrium; Q_t (mg g^{-1}) is the amount of dye adsorbed at any time t (min); k_2 (g mg^{-1} min^{-1}) is the second-order rate constant [33]; K_T (mg g^{-1}·$min^{1/2}$) is the diffusion rate constant [34]; C is a constant related to the thickness of boundary layer [34]; a (mg g^{-1} min^{-1}) is the initial sorption rate [35]; b (g mg^{-1}) is the desorption constant related to the extent of surface coverage and activation energy for chemisorption [35].

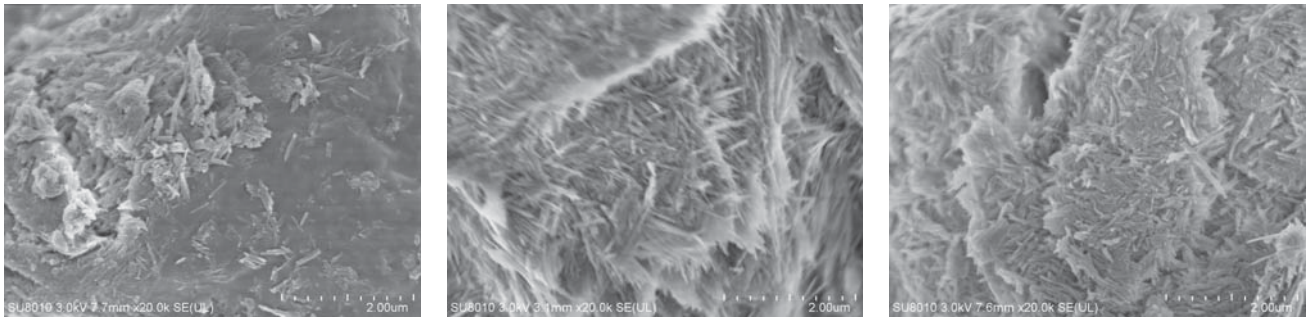

(a) (b) (c)

Figure 8: The surface morphology of the nanocomposite particles ((a) AC1; (b) AC2; (c) AC3).

Table 1: Kinetic models and their equations.

Kinetic model	Equation	Plot	Reference
Pseudo-first-order	$\log(Q_{eq} - Q_t) = \log Q_{eq} - k_1 t$	$\log(Q_{eq} - Q_t)$ versus t	[32]
Pseudo-second-order	$\frac{t}{Q_t} = \frac{1}{k_2 Q_{eq}^2} + \frac{1}{Q_{eq}} t$	t/Q_t versus t	[33]
Intraparticle diffusion	$Q_t = K_T t^{1/2} + C$	Q_t versus t	[34]
Elovich equation	$Q_t = \left(\frac{1}{b}\right) \ln(ab) + \frac{1}{b} \ln t$	Q_t versus $\ln t$	[35]

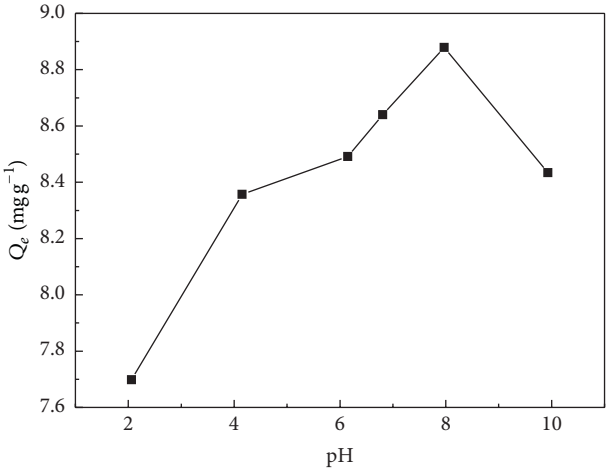

Figure 9: The influence of pH on the adsorption capacity of AC2 for methylene blue with concentration of 12.016 mg L^{-1} at 25°C.

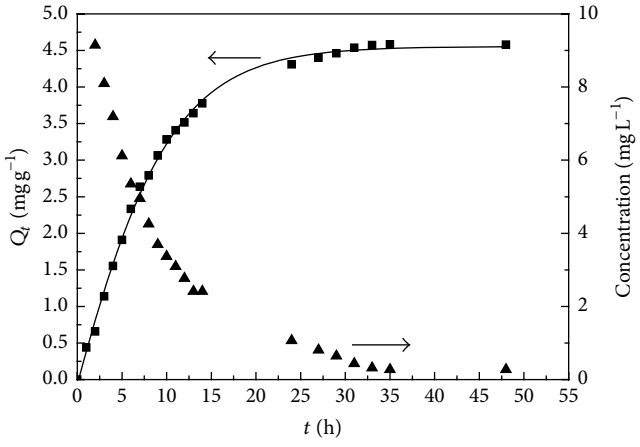

Figure 10: The absorbed capacity of AC1 for methylene blue with concentration of 12.016 mg L^{-1} at 25°C and pH = 7.0 as a function of time (■ represents experiment data; the full line represents fit of experimental data with a pseudo-first-order kinetic equation; ▲ represents concentration of methylene blue in solution).

The pseudo-second-order model assumes that the rate limiting step is chemical sorption [36]. Elovich model recently has been found to be valid to describe the sorption kinetics of ion exchange systems [18]. The fitted parameters of these kinetic models are listed in Table 2. R^2 of the linear form for the various models suggests that the pseudo-first-order model is more suitable to describe the adsorption kinetic behavior. Using intraparticle diffusion model, plots of Q_t versus $t^{1/2}$ do not pass through the origin indicating that the adsorption process is also controlled by film diffusion [36].

3.6. Adsorption Equilibrium Study. The equilibrium adsorption data is shown in Figure 11. At each temperature, adsorption capacity of AC2 for five different concentrations of methylene blue was measured. The equilibrium adsorption data was correlated to four isotherm models: Langmuir [37], Freundlich [38], Sips [39], and Dubinin-Radushkevich [40]. Table 3 shows the equations of these models. In these models, Q_{max} is the maximum adsorption at monolayer coverage (mg g^{-1}) [37]; b is equilibrium constant (mL mg^{-1}) in Langmuir adsorption [37] or Sips constant related to energy of adsorption in Sips model [39]; K_F is the Freundlich characteristic constants [38]; $1/n$ is the Freundlich characteristic constants [38]; n could be regarded as the Sips parameter characterizing the system heterogeneity; B is a constant

Table 2: The kinetic parameters for MB adsorption onto AC1.

T (°C)	Pseudo-first-order equation		Pseudo-second-order equation		Intraparticle diffusion models		Elovich equation		
	k_1 (min^{-1})	R^2	k_2 (g mg^{-1} min^{-1})	R^2	K_T (mg g^{-1} $min^{-1/2}$)	R^2	a (mg g^{-1} min^{-1})	b (g mg^{-1})	R^2
25	0.11309	0.9952	0.01674	0.9779	0.7593	0.8746	1.3717	0.7705	0.9687

Table 3: Isotherm models and their equations.

Isotherm model	Equation	Plot	Reference
Langmuir	$\frac{1}{Q_{eq}} = \frac{1}{Q_{max}} + \frac{1}{Q_{max}b}\frac{1}{C_e}$	$1/Q_{eq}$ versus $1/C_e$	[37]
Freundlich	$\ln Q_{eq} = \frac{1}{n}\ln C_e + \ln K_F$	$\ln Q_{eq}$ versus $\ln C_e$	[38]
Sips	$Q_{eq} = \frac{Q_m b C_e^{1/n}}{1 + bC_e^{1/n}}$	Q_{eq} versus C_e	[39]
Dubinin-Radushkevich	$\ln Q_{eq} = \ln Q_m - B\varepsilon^2$	$\ln Q_{eq}$ versus ε	[40]

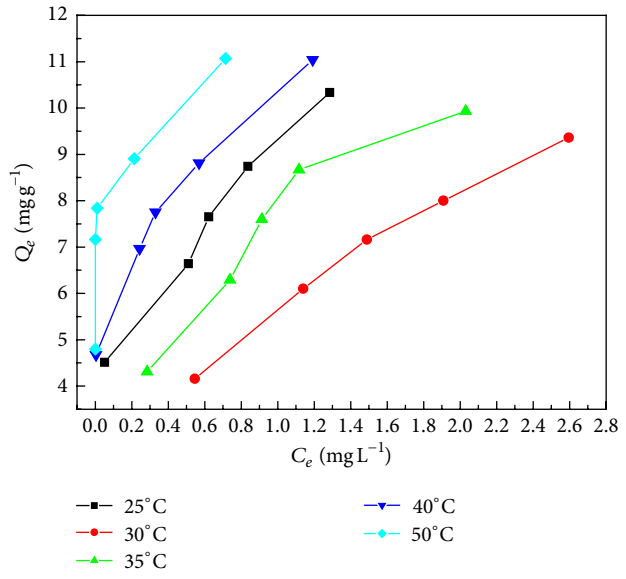

Figure 11: The curve of C_e-Q_e of AC2 under different temperatures with duration time of 36 h.

related to the mean free energy of adsorption per mol of the adsorbate (mol^2 J^{-2}) [40]; Q_m is the theoretical saturation capacity (mg g^{-1}) [40]; ε is the Polanyi potential [40], which is equal to $RT\ln(1+1/C_e)$; R (J mol^{-1} K^{-1}) is the gas constant; T (K) is the absolute temperature.

The Langmuir isotherm model assumes the adsorption is monolayer adsorption [18]. A finite number of identical sites exist on a surface and all sites are energetically equivalent and there is no interaction between adsorbed molecules. Freundlich model is applied to describe that adsorption occurs on a heterogeneous surface. The fitting parameters of the above models are listed in Table 4. Most of the determination coefficients (R^2) of the Langmuir model exceed 0.93 compared with those of the other models. This indicates that the Langmuir model is suitable to describe the adsorption behavior of AC2. So it can be concluded that methylene blue molecule is absorbed on the surface with monolayer. From Figure 11, we can see that C_e is almost near zero at 25°C, 40°C, and 50°C, which indicates that the particle can remove dye in very dilute aqueous solutions.

3.7. Regeneration Efficiency. Reusability is very important for adsorbent in practical applications. In current work, the adsorption and desorption processes were repeated for three cycles to measure the regeneration efficiency. 0.1 mol L^{-1} H_2SO_4 aqueous solution was used to recover the methylene blue loaded composite particles. Table 5 shows the adsorption capacities and the regeneration efficiency in each cycle. After three cycles, AC2 gets 94.64% recovery, indicating a high regeneration efficiency. This also illuminates that the adsorbent is suitable for practical applications.

4. Conclusions

The attapulgite nanofibers were coated onto the surface of cellulose bead to form nanocomposite particles with core-shell structure. SEM, FTIR, XRD, and TG all revealed that attapulgite nanofiber exists in the shell of nanocomposite particles. Nanocomposite particles have higher adsorption capacity than cellulose bead. Adsorption capacity is changed with pH of dye solution and largest adsorption capacity occurs at pH = 8. The adsorption equilibrium and kinetics study of composite particles indicate that the adsorption behavior follows Langmuir model and pseudo-first-order equation. Dye-loaded nanocomposite could be regenerated easily and high adsorption ability is reserved. Simple preparation, low cost, being easy to regenerate make the core-shell structured nanocomposite a suitable carrier for attapulgite and an attractive adsorbent for removal of the organic dyes from water. This study also proposes a new approach to use the attapulgite and cellulose as adsorption material.

Table 4: The isotherms parameters for methylene blue adsorption onto AC2.

T (°C)	Langmuir model			Freundlich model			Dubinin-Radushkevich model			Sips model			
	Q_{max} (mg g^{-1})	b (L mg^{-1})	R^2	$1/n$	K_F (mg g^{-1})	R^2	Q_{max} (mg g^{-1})	E (kJ/mol)	R^2	Q_{max} (mg g^{-1})	b	$1/n$	R^2
25	11.2284	4.6800	0.9365	0.2410	8.8710	0.9282	8.7615	6.3976	0.8012	123.1803	0.0795	0.2963	0.9153
30	14.1965	0.7031	0.9875	0.5227	5.7221	0.9991	9.1354	2.0422	0.9360	51.6949	0.1252	0.5965	0.9992
35	13.1130	1.5313	0.9801	0.4446	7.6222	0.9677	9.6025	2.9773	0.9125	16.70934	0.8786	0.7696	0.9677
40	11.6023	8.7149	0.9721	0.1413	9.4353	0.9199	8.8507	12.1932	0.7702	151.0619	0.0699	0.1783	0.9006
50	11.3469	36.8745	0.9940	0.0741	10.7578	0.8544	10.2382	16.4501	0.7087	320.9413	0.0351	0.0818	0.8492

Table 5: Adsorption-desorption cycles of methylene blue.

Sample	Adsorption ability	First adsorption	Second adsorption	Third adsorption	Fourth adsorption
AC1	Adsorption capacity (mg g^{-1})	8.6317	8.5228	7.9651	7.6254
	Recovery (%)	—	98.74	92.28	88.34
AC2	Adsorption capacity (mg g^{-1})	8.7754	8.6317	8.5707	8.3050
	Recovery (%)	—	98.36	97.67	94.64

Competing Interests

The authors declare that they have no competing interests.

Acknowledgments

The authors would like to thank the Natural Science Foundation for Colleges and Universities of Jiangsu Province (Grant no. 12KJD150006) for the financial support of this research.

References

[1] Y. Liu, P. Liu, Z. Su, F. Li, and F. Wen, "Attapulgite-Fe_3O_4 magnetic nanoparticles via co-precipitation technique," *Applied Surface Science*, vol. 255, no. 5, pp. 2020–2025, 2008.

[2] W. B. Wang and A. Q. Wang, "Nanocomposite of carboxymethyl cellulose and attapulgite as a novel pH-sensitive superabsorbent: synthesis, characterization and properties," *Carbohydrate Polymers*, vol. 82, no. 1, pp. 83–91, 2010.

[3] B. Mu, Q. Wang, and A. Q. Wang, "Preparation of magnetic attapulgite nanocomposite for the adsorption of Ag^+ and application for catalytic reduction of 4-nitrophenol," *Journal of Materials Chemistry A*, vol. 1, no. 24, pp. 7083–7090, 2013.

[4] Y. Liu, W. B. Wang, Y. L. Jin, and A. Q. Wang, "Adsorption behavior of methylene blue from aqueous solution by the hydrogel composites based on attapulgite," *Separation Science and Technology*, vol. 46, no. 5, pp. 858–868, 2011.

[5] L. Wang, J. P. Zhang, and A. Q. Wang, "Fast removal of methylene blue from aqueous solution by adsorption onto chitosan-g-poly (acrylic acid)/attapulgite composite," *Desalination*, vol. 266, no. 1–3, pp. 33–39, 2011.

[6] Q.-H. Fan, P. Li, Y.-F. Chen, and W.-S. Wu, "Preparation and application of attapulgite/iron oxide magnetic composites for the removal of U(VI) from aqueous solution," *Journal of Hazardous Materials*, vol. 192, no. 3, pp. 1851–1859, 2011.

[7] M. Alexandre and P. Dubois, "Polymer-layered silicate nanocomposites: preparation, properties and uses of a new class of materials," *Materials Science and Engineering R: Reports*, vol. 28, no. 1, pp. 1–63, 2000.

[8] K. Kabiri, H. Omidian, M. J. Zohuriaan-Mehr, and S. Doroudiani, "Superabsorbent hydrogel composites and nanocomposites: a review," *Polymer Composites*, vol. 32, no. 2, pp. 277–289, 2011.

[9] M. Shibayama, "Structure-mechanical property relationship of tough hydrogels," *Soft Matter*, vol. 8, no. 31, pp. 8030–8038, 2012.

[10] H. X. Yang, W. B. Wang, and A. Q. Wang, "A pH-sensitive biopolymer-based superabsorbent nanocomposite from sodium alginate and attapulgite: synthesis, characterization, and swelling behaviors," *Journal of Dispersion Science and Technology*, vol. 33, no. 8, pp. 1154–1162, 2012.

[11] P. Liu, L. P. Jiang, L. X. Zhu, and A. Q. Wang, "Attapulgite/poly(acrylic acid) nanocomposite (ATP/PAA) hydrogels with multifunctionalized attapulgite (org-ATP) nanorods as unique cross-linker: preparation optimization and selective adsorption of Pb(II) Ion," *ACS Sustainable Chemistry and Engineering*, vol. 2, no. 4, pp. 643–651, 2014.

[12] M. Zhang, J. Soto-Rodríguez, I.-C. Chen, and M. Akbulut, "Adsorption and removal dynamics of polymeric micellar nanocarriers loaded with a therapeutic agent on silica surfaces," *Soft Matter*, vol. 9, no. 42, pp. 10155–10164, 2013.

[13] I.-C. Chen, M. Zhang, B. Teipel, I. S. De Araujo, Y. Yegin, and M. Akbulut, "Transport of polymeric nanoparticulate drug delivery systems in the proximity of silica and sand," *Environmental Science and Technology*, vol. 49, no. 6, pp. 3575–3583, 2015.

[14] S. Liu, D. Tao, T. Yu, H. Shu, R. Liu, and X. Liu, "Highly flexible, transparent cellulose composite films used in UV imprint lithography," *Cellulose*, vol. 20, no. 2, pp. 907–918, 2013.

[15] M. Zhang and M. Akbulut, "Adsorption, desorption, and removal of polymeric nanomedicine on and from cellulose surfaces: effect of size," *Langmuir*, vol. 27, no. 20, pp. 12550–12559, 2011.

[16] J. Zhou, C. Chang, R. Zhang, and L. Zhang, "Hydrogels prepared from unsubstituted cellulose in NaOH/urea aqueous solution," *Macromolecular Bioscience*, vol. 7, no. 6, pp. 804–809, 2007.

[17] J. Cai, L. Zhang, J. Zhou et al., "Multifilament fibers based on dissolution of cellulose in NaOH/urea aqueous solution:

structure and properties," *Advanced Materials*, vol. 19, no. 6, pp. 821–825, 2007.

[18] W. X. Zhang, H. Yang, L. Dong et al., "Efficient removal of both cationic and anionic dyes from aqueous solutions using a novel amphoteric straw-based adsorbent," *Carbohydrate Polymers*, vol. 90, no. 2, pp. 887–893, 2012.

[19] J. Han, Z. Zhou, R. Yin, D. Yang, and J. Nie, "Alginate-chitosan/hydroxyapatite polyelectrolyte complex porous scaffolds: preparation and characterization," *International Journal of Biological Macromolecules*, vol. 46, no. 2, pp. 199–205, 2010.

[20] J.-H. Huang, Y.-F. Liu, Q.-Z. Jin, and X.-G. Wang, "Spectra study on the influence of drying process on palygorskite structure," *Spectroscopy and Spectral Analysis*, vol. 27, no. 2, pp. 408–410, 2007.

[21] Z. Lei, Q. Yang, S. Wu, and X. Song, "Reinforcement of polyurethane/epoxy interpenetrating network nanocomposites with an organically modified palygorskite," *Journal of Applied Polymer Science*, vol. 111, no. 6, pp. 3150–3162, 2009.

[22] C. Wang, Q. Wu, F. Liu et al., "Synthesis and characterization of soy polyol-based polyurethane nanocomposites reinforced with silylated palygorskite," *Applied Clay Science*, vol. 101, pp. 246–252, 2014.

[23] W. Li, A. Adams, J. D. Wang, B. Blümich, and Y. G. Yang, "Polyethylene/palygorskite nanocomposites: preparation by in situ polymerization and their characterization," *Polymer*, vol. 51, no. 21, pp. 4686–4697, 2010.

[24] Y. Zhang, W. Wang, J. Zhang, P. Liu, and A. Wang, "A comparative study about adsorption of natural palygorskite for methylene blue," *Chemical Engineering Journal*, vol. 262, pp. 390–398, 2015.

[25] Y. Liu, W. Wang, and A. Wang, "Adsorption of lead ions from aqueous solution by using carboxymethyl cellulose-g-poly (acrylic acid)/attapulgite hydrogel composites," *Desalination*, vol. 259, no. 1–3, pp. 258–264, 2010.

[26] L. Guo, G. Y. Li, J. S. Liu, Y. F. Meng, and Y. F. Tang, "Adsorptive decolorization of methylene blue by crosslinked porous starch," *Carbohydrate Polymers*, vol. 93, no. 2, pp. 374–379, 2013.

[27] M. S. U. Rehman, I. Kim, and J.-I. Han, "Adsorption of methylene blue dye from aqueous solution by sugar extracted spent rice biomass," *Carbohydrate Polymers*, vol. 90, no. 3, pp. 1314–1322, 2012.

[28] A. Al-Futaisi, A. Jamrah, A. Al-Rawas, and S. Al-Hanai, "Adsorption capacity and mineralogical and physico-chemical characteristics of Shuwaymiyah palygorskite (Oman)," *Environmental Geology*, vol. 51, no. 8, pp. 1317–1327, 2007.

[29] G. Y. Tian, Y. R. Kang, B. Mu, and A. Q. Wang, "Attapulgite modified with silane coupling agent for phosphorus adsorption and deep bleaching of refined palm oil," *Adsorption Science & Technology*, vol. 32, no. 1, pp. 37–48, 2014.

[30] H. Chen and J. Zhao, "Adsorption study for removal of Congo red anionic dye using organo-attapulgite," *Adsorption*, vol. 15, no. 4, pp. 381–389, 2009.

[31] M. T. Yagub, T. K. Sen, and M. Ang, "Removal of cationic dye methylene blue (MB) from aqueous solution by ground raw and base modified pine cone powder," *Environmental Earth Sciences*, vol. 71, no. 4, pp. 1507–1519, 2014.

[32] S. Lagergren, "About the theory of so-called adsorption of soluble substances," *Kungliga Svenska Vetenskapsakademiens Handlingar*, vol. 24, pp. 1–39, 1898.

[33] Y. S. Ho and G. McKay, "Sorption of dye from aqueous solution by peat," *Chemical Engineering Journal*, vol. 70, no. 2, pp. 115–124, 1998.

[34] Y. A. Yahaya, M. Mat Don, and S. Bhatia, "Biosorption of copper (II) onto immobilized cells of Pycnoporus sanguineus from aqueous solution: equilibrium and kinetic studies," *Journal of Hazardous Materials*, vol. 161, no. 1, pp. 189–195, 2009.

[35] M. J. D. Low, "Kinetics of chemisorption of gases on solids," *Chemical Reviews*, vol. 60, no. 3, pp. 267–312, 1960.

[36] C. Duran, D. Ozdes, A. Gundogdu, and H. B. Senturk, "Kinetics and isotherm analysis of basic dyes adsorption onto almond shell (*Prunus dulcis*) as a low cost adsorbent," *Journal of Chemical & Engineering Data*, vol. 56, no. 5, pp. 2136–2147, 2011.

[37] I. Langmuir, "The adsorption of gases on plane surfaces of glass, mica and platinum," *The Journal of the American Chemical Society*, vol. 40, no. 9, pp. 1361–1403, 1918.

[38] H. M. F. Freundlich, "Über die adsorption in lösungen," *Zeitschrift für Physikalische Chemie*, vol. 57, pp. 385–470, 1906.

[39] R. Sips, "On the structure of a catalyst surface," *The Journal of Chemical Physics*, vol. 16, no. 5, pp. 490–495, 1948.

[40] M. M. Dubinin, "Sorption and structure of active carbons: I. Adsorption of organic vapors," *Zhurnal Fizicheskoi Khimii*, vol. 21, pp. 1351–1362, 1947.